IEEE Access
Multidisciplinary | Rapid Review | Open Access Journal

Received 11 December 2023, accepted 25 December 2023, date of publication 8 January 2024,
date of current version 19 January 2024.

Digital Object Identifier 10.1109/ACCESS.2024.3351354

RESEARCH ARTICLE

Diversified Intelligent Terminal Devices Unified Access and Data Communication Technology

XUEYAN WANG, HONGLIANG ZOU, HAIBO LI, HEMING QIAN, AND XINYI HE
State Grid Zhejiang Electric Power Supply Company, Taizhou Branch, Taizhou 317700, China
Corresponding author: Heming Qian (qianheming987@163.com)

ABSTRACT Different intelligent devices have different operating systems, data interaction modes and network connection modes, which greatly hinder the realization of the Internet of everything. In view of the above problems, the combination of multi-IP core and Internet of Things application server, and the field programmable door array to improve its response speed, and reduce the system power consumption. Then a set of data communication technology is designed on the basis of Huffman coding to improve the data compression efficiency of the system and adapt to the transmission of various data. The experimental results show that the propagation efficiency of this data communication technology is about 73% on average, and the transmission rate fluctuates between 8MB and 14MB per second, which can reduce the coding time by about 10% compared with the traditional Huffman coding.

INDEX TERMS Intelligent terminal, Internet of Things, data communication technology, multiple IP cores, field programmable gate srray.

I. INTRODUCTION

With the continuous progress of science and technology and the flourishing development of digitalization, interconnected IT equipment has become an indispensable part of modern society [1]. However, the challenges and complexities of connecting different IT devices are also emerging. This paper will explore in detail the challenges and complexities of connecting different IT devices and clarify why these challenges are critical to users and the digital ecosystem [2], [3]. First, connecting different IT devices involves differences between different operating systems, communication protocols, and data formats. For example, the operating system used by a smartphone may be different from that used by smart home devices or industrial automation devices [4]. This difference leads to interoperability problems between devices, making it difficult for users to achieve seamless device connectivity and collaborative work. Secondly, different devices use different communication protocols, such as Wi-Fi, Bluetooth, Zigbee, etc. Incompatibility between these protocols makes communication between devices difficult, requiring adaptation and conversion. In addition, communication between devices may be affected by signal interference, distance limitations, and security and privacy protection. In addition, different devices use different data formats to store and represent the data. This difference in data format makes transferring and interpreting data between devices complicated [5]. In addition, data security and privacy issues are also important factors to consider when connecting to different devices. These challenges and complexities have important implications for users and digital ecosystems. For users, the difficulty of connecting different IT devices may lead to a decreased use experience and reduced user satisfaction. Users may have to face problems where devices cannot work with each other, and data cannot be shared and transmitted. But these technologies are not enough to solve the complexity of connecting different devices and the performance problems.In view of this, the study first adopted the field programmable gate array (Field-Programmable Gate Array, FPGA), combined with the multi-IP core and Internet of Things application server to design the multi-IP core Internet of Things application server (Multiple IP cores-Internet of Things Application Server, MIC-IoTAS), and then proposed a series of optimization measures to improve the access capacity of the system. On the basis of Huffman coding, combined efficient video coding (High Efficiency Video Coding, HEVC)

The associate editor coordinating the review of this manuscript and approving it for publication was Tawfik Al-Hadhrami.

and DCT transformation (Discrete Cosine Transform, DCT) (Joint Huffman Coded Discrete Cosine Transform, JHC-DCT). The research aims to explore and study the unified access and data communication technology of diversified terminal devices and improve the performance of terminal devices, so as to contribute to the building of a seamless connected and interconnected digital ecosystem.The research mainly includes four parts. The second part summarizes the current research status of IoT and DC technology, and summarizes the research achievements and methods at home and abroad. Thirdly, a diversified IT unified access model and DC technology were designed, and JHC-DCT network communication scheme and MIC-IoTAS terminal access scheme were established. Finally, the optimization effect of the model was evaluated through comparative experiments and efficiency validation. The performance of this technology has been tested in various aspects in practical use.

II. RELATED WORKS

The arrival of IoT has led more people to attach importance to the interconnection of diverse IT, and DC technology has made significant progress. The rapid growth of data traffic in the communication industry has led to excessive network load. In response, Ren et al. designed an emerging semiconductor material that can provide tunable optoelectronic properties and solution processability. These experiments confirm that the material improves the modulation performance and device efficiency of LEDs [6]. Aceto et al. explored a network framework that combines mobile computing and human-computer interaction to address the complexity of network communication technology in the Industry 4.0 process. These experiments confirm that the framework improves overall network performance [7]. Poulton et al. has designed a long-range LiDAR with high-performance optical phased array and free space DC technology to improve the performance of DC. These results confirm that this technology significantly improves data transmission performance [8]. Wang et al. have designed a secure vehicle DC method based on NDN to address the safety issues of on-board DCs. These experiments confirm that this method reduces DC costs and failure rates [9]. Sekera et al. proposed a method for connecting low Earth orbit satellites to the Internet to address the difficulties of space and aviation DC. These experiments confirm that this method improves the reliability of aerospace communication systems [10]. Kholit and other scholars have designed three dissemination network models to address the problem of the proliferation of false information on the Internet, namely centralized network, decentralized network, and distributed network. These results confirm that this method reduces the spread of false information on the internet [11].

Emroozi et al. designed a new supply chain design based on IoT and delivery reliability to address waste and returns in the supply chain system. These experiments confirm that the supply chain using this system has reduced waste by 20% [12]. To explore the potential of IoT, Kumar et al. discussed different challenges and key issues in IoT, architecture, and important application areas. This helps readers and researchers understand IoT and its applicability in the real world [13]. Alsharari et al. designed a new blockchain trading technology by combining blockchain with IoT to improvetrading accuracy. These results confirm that the technology improves the integration efficiency of these two [14]. Singh and other scholars have designed an IoT based medical security system to improve patient satisfaction and reduce readmission rates in hospitals. These results confirm that the system reduces the operating costs of the medical system [15]. Liu et al. designed a new security mechanism by combining IoT and machine learning to address many security issues in IoT devices. These results confirm that this method improves system security by 42% [16]. Xie et al. proposed a DL based-lite distributed semantic communication system, L-DeepSC, to address the issue of limited computing power and difficulty in achieving semantic communication in IoT devices, for low complexity text transmission. These experiments confirm that the system performs well in low signal-to-noise ratio regions, achieving a compression ratio of 40% [17].

In summary, DC and unified access between diversified intelligent devices have become important means to achieve IoT. However, the traditional DC method lacks consideration in terms of video data compression and security. Therefore, the study combines MIC and IoTAS, and designs a more efficient and secure DC technology based on Huffman encoding in conjunction with HEVCDCT to promote the IoT industry.

III. DESIGN OF UNIFIED ACCESS TECHNOLOGY FOR IT EQUIPMENT AND DC TECHNOLOGY

This chapter consists of two parts. Firstly, a unified access scheme for MIC-IoTAS devices is designed based on the use of FPGA, combining MIC and IoTAS. Secondly, based on Huffman encoding, a DC technology was designed in conjunction with HEVCDCT.

A. MIC-IOTAS EXTENSION ACCESS INTERFACE

The core module of the architecture is mainly implemented based on IP cores, which include user-defined IP cores and third-party IP cores. Among them, user-defined IP cores are reusable components developed based on specific needs, while third-party IP cores are mature and validated modules provided by external suppliers. Adopting IP core development and reuse technology can significantly reduce the difficulty and cycle of system development, and ensure that the system can be quickly implemented. By utilizing existing IP cores, developers can avoid designing and implementing all functional modules from scratch, thereby saving a lot of time and effort. In addition, the reusability of IP cores also enables the system to migrate and share more efficiently between different projects, further improving development efficiency. On the other hand, based on various verified IP cores, the system can be guaranteed to have good stability and reliability. By extending the IoTAS access interface, external devices can send data to the IoTAS platform, receive

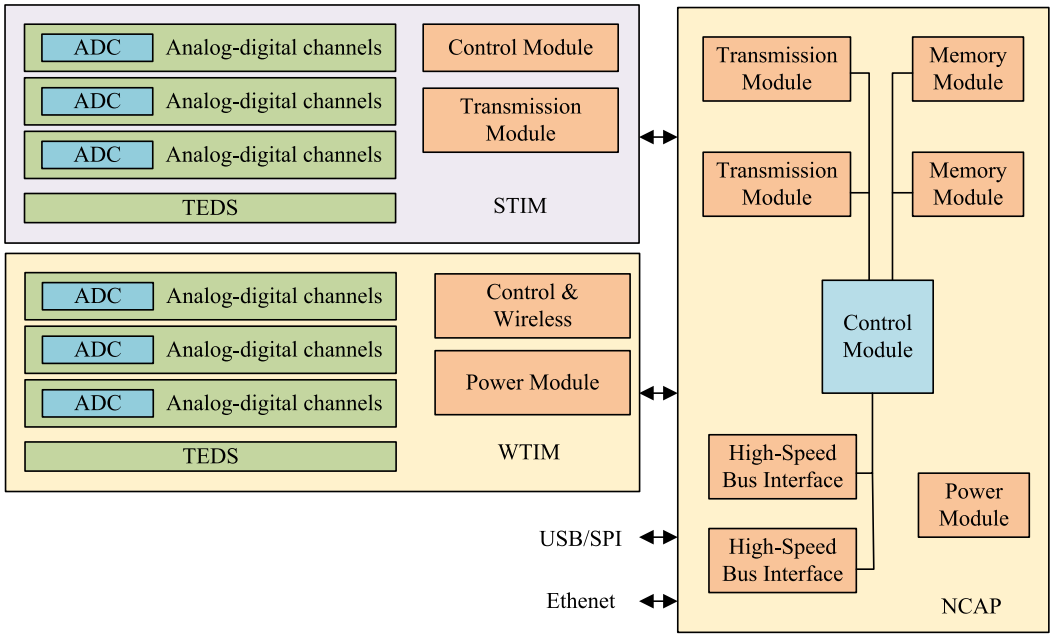

FIGURE 1. Schematic diagram of MIC-IoTAS model structure.

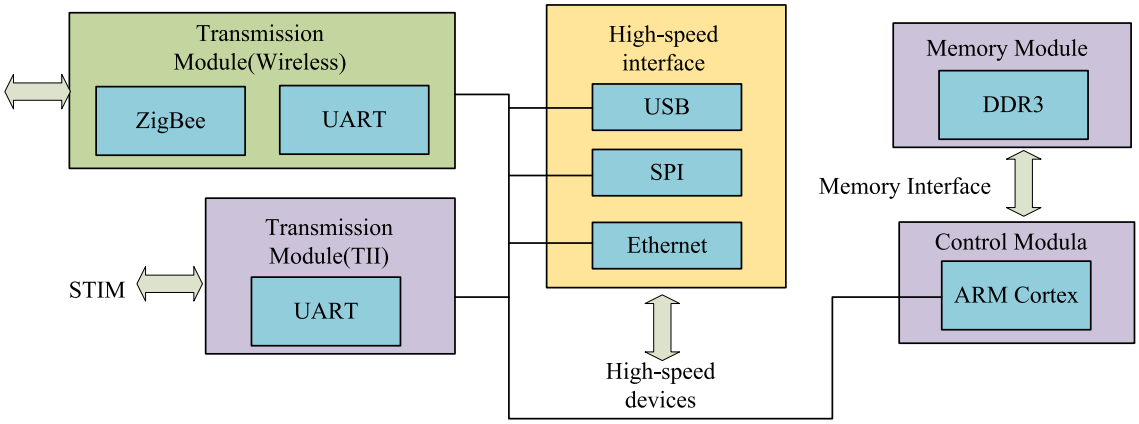

FIGURE 2. Schematic diagram of NCAP model structure.

commands, and communicate with other devices and services on the platform. In this way, the IoTAS platform can serve as a central hub to integrate and manage multiple different types of devices and systems, achieving data aggregation, analysis, and control. The IoTAS extension access interface provides a consistent data model, message format, and protocol specification to ensure seamless integration of various external devices and systems with the IoTAS platform. It simplifies the work of developers, reduces the complexity of integration, and promotes interoperability between different vendors and technologies. In IoTAS, multiple IP cores can be combined and integrated to achieve different types of access interface functions. These IP cores can include Ethernet controllers, serial interfaces, wireless communication modules, etc., and can be selected and configured according to specific needs. MIC-IoTAS model is formed by integrating multiple IP cores into IoTAS system in Figure 1.

In the entire architecture, Networked Control and Automation Platform (NCAP) serves as the "computing management hub" of the system, responsible for the core computing, storage, and management work of the system. Through communication with other devices and systems, it achieves data collection, processing, and analysis. NCAP, as a centralized control node, is responsible for coordinating and managing various components and functional modules of the entire system, ensuring system stability and efficiency. It provides a unified interface and protocol, allowing different types of devices and systems to seamlessly interact and integrate with it, thereby achieving intelligent control and automated management. NCAP can meet the requirements of system

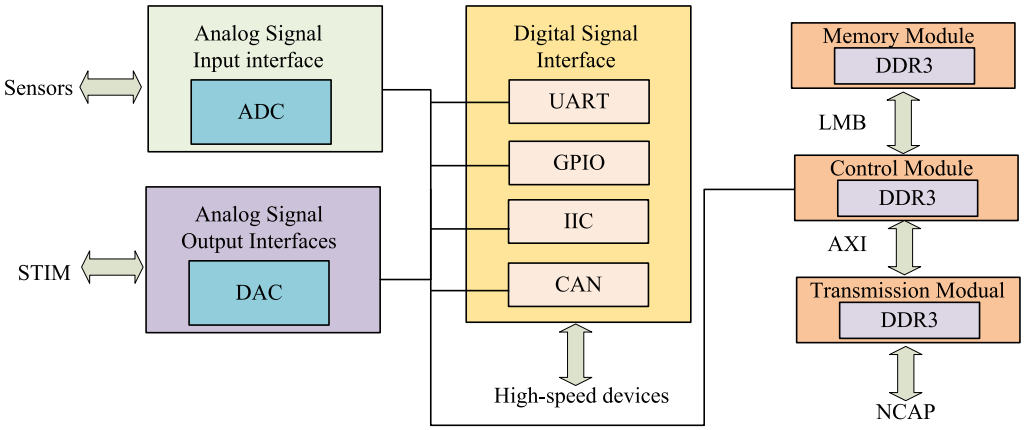

FIGURE 3. Schematic diagram of STIM model structure.

well and provide reliable data transmission and processing capabilities, providing strong computing and management support for the entire system in Figure 2.

Sensor and Transformer Interface Module (STIM) is the ''wired acquisition hub'' of the system, responsible for accessing low-speed devices such as sensors and actuators. STIM utilizes Analog to Digital Converter (ADC) to achieve access support for analog output interface devices. The analog signals output by the device are converted into digital signals through ADC, which can be further analyzed and processed by the system. STIM, as a key component of this system, is responsible for connecting various types of sensors and actuators with the system to provide accurate data collection and control functions. STIM can ensure the interoperability and universality of devices, and seamlessly integrate with other devices that meet this standard, thereby achieving efficient and reliable data acquisition and signal conversion processesin Figure 3.

WTIM (Wireless Transducer Interface Module) is the ''wireless acquisition center'' of the system, which is responsible for wireless access to low-speed devices such as sensors and actuators. WTIM uses wireless communication technologies, such as Wi-Fi, Bluetooth or Zigbee, to wirelessly connect with sensor devices to achieve data transmission and remote control. With the help of wireless acquisition center, the limitation of wired connection can be eliminated and provide greater flexibility and convenience. The overall architecture of the entire IoTAS extended access interface can effectively support the unified hardware access of massive heterogeneous devices under the Internet of Things. This includes not only low-speed devices such as traditional sensors and actuators, but also new and high-speed devices such as digital cameras and printers. This integrated architecture ensures seamless device connectivity and interoperation with the IoTAS platform by providing diverse interfaces and protocol support. The presence of WTIM can reduce the computing and communication burden of terminal devices. For example, a terminal device simply needs to send data to WTIM without communicating directly with the cloud or the main controller. This approach of ''uninstalling'' computing tasks to WTIM helps to improve terminal device performance and battery life. In addition, combined with technologies such as the Field Programmable Door Array (FPGA), WTIM can support new and high-speed devices at a lower cost of hardware resources. The programmability of FPGA enables WTIM to flexibly adapt to different device interfaces and protocols, thus further improving the utilization efficiency of hardware resources. It is a programmable logic device, as shown in Figure 4.

Unlike traditional fixed function integrated circuits, FPGA can achieve specific digital logic functions through programming. It consists of a series of programmable logical blocks and programmable connection resources [18]. FPGA has flexibility and reconfigurability, allowing engineers to configure and modify its logical functions as needed. This means that FPGA can be used to implement various digital circuits, including processors, memory, counters, multipliers, etc., [19], [20], [21]. By reprogramming the FPGA, designers can quickly prototype and validate the design, and iterate and optimize it during the design process.In order to enhance the access capabilities of STIM and WTIM, a series of comprehensive and detailed hardware improvement and software optimization plans need to be taken. For hardware improvements, STIM can increase the number of ADC channels to support more sensor access and increase the ADC sampling rate to obtain more accurate signals. In addition, in order to adapt to different types of sensor outputs, it is also necessary to consider increasing the analog input voltage range of STIM. For WTIM, introduce faster wireless communication technologies such as 5G or Wi Fi 6 to ensure communication with external devices is maintained at high speed and low latency. At the same time, increasing the number and diversity of antennas can improve the stability and coverage of wireless communication. In terms of software and algorithms, STIM can optimize data processing algorithms to process and forward data to NCAP at a faster speed. Develop adaptive sensor recognition algorithms to enable STIM to automatically

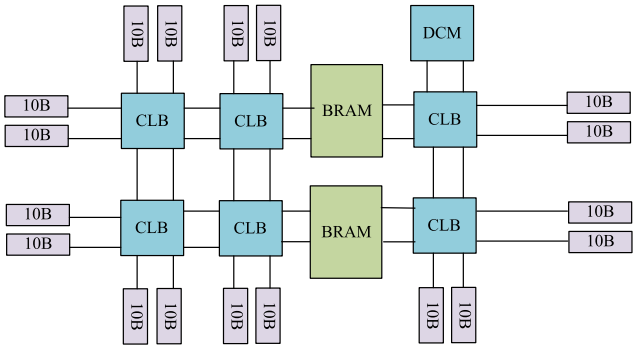

FIGURE 4. FPGA schematic diagram.

recognize sensor types and adaptively adjust parameters such as sampling rate and gain. In addition, the introduction of priority management mechanism can schedule based on the priority of sensors or the importance of data, ensuring the priority processing of critical data. For the software and protocol optimization of WTIM, firstly, optimize the wireless access protocol, remove unnecessary functions and steps through protocol stack pruning, making it more concise and efficient. Introduce a fast connection mechanism to reduce the number of signaling interactions during the connection establishment process, enabling devices to quickly establish connections with WTIM. At the same time, improve the protocol to support simultaneous access of multiple devices, avoid access conflicts, and reduce retransmission probability. Secondly, implement concurrent connection management by designing connection queue management to manage the attempted devices, and dynamically adjust the position of devices in the queue based on factors such as device priority and historical connection records. Introduce a load balancing mechanism to evenly allocate concurrent connections to multiple processing units, ensuring that each connection can be processed in a timely manner. At the same time, a connection timeout management mechanism is established to automatically release connections without data interaction for a long time, effectively releasing resources for new device access. Finally, in order to ensure the efficiency and security of data transmission, we can adopt a series of technical solutions. By monitoring signal strength and detecting factors such as mobility, the data transmission rate is dynamically adjusted to achieve adaptive rate adjustment. In terms of data compression and encryption, choose efficient compression algorithms and mature encryption schemes, and design collaborative processing mechanisms to enable data to be encrypted immediately after compression and then transmitted. This can save bandwidth while ensuring data security.

B. DC TECHNIQUE FOR HEVCDCT COEFFICIENTS USING JHC

After addressing the issue of unified IT access, it is also necessary to address the intermediate DC issue. The solution to DC involves multiple aspects, first of all, the transmission medium, which DC needs to carry the transmission of information. The transmission medium can be wired, such as copper cable, optical fiber, etc. It can also be wireless, such as radio waves and microwaves. Secondly, there are protocols and standards. In DC, protocols and standards specify the format of data, transmission methods, error detection and correction mechanisms, and data frame structure. Common network protocols include TCP/IP, HTTP, FTP, etc. Then there is the modem, which converts the digital signal into an analog signal for propagation through the transmission medium, while also converting the received analog signal into a digital signal. Modems play an important role in wired and wireless communication, and wireless communication technologies include Bluetooth, Wi Fi, mobile communication (such as 3G, 4G, 5G), IoT communication protocols, etc. [22]. These technologies enable TD to transmit and communicate data wirelessly. In addition, security in DC is also very important, especially when it comes to confidential information or sensitive data. Data security and encryption technologies are used to protect the privacy and integrity of data, preventing unauthorized access and tampering. Data compression is a processing method that converts data representation into a more compact form to reduce storage space or reduce the cost of data transmission during data exchange. Data compression can be used in multiple fields and applications, such as data storage, data transmission, image processing, audio processing, etc. The following process can be used to compress data from different IT sources in Figure 5.

Figure 5 shows the process of compressing data from different IT sources. Firstly, data collection is carried out to obtain data from various IT sources, including text, images, audio, video, and other forms of data. Then there is data preprocessing, which preprocesses the original data, such as removing noise, reducing redundancy, standardizing, etc., to improve the data compression effect. The third step is to select a compression algorithm based on the data type and characteristics. Next is data compression, which applies the selected compression algorithm to each data block and converts it into smaller representations. This may involve operations such as encoding, transformation, quantization, etc., depending on the selected compression algorithm. Then, a compression ratio calculation was conducted to evaluate the compression effect by calculating the compression ratio of the compressed data relative to the original data. The sixth step is data transmission/storage, which transfers the compressed data to the target system or storage device. It can be transmitted and stored on cloud or local devices through the network, and suitable methods can be selected according to needs. Finally, there is decompression, which decompresses the compressed data on the target system and restores it to its original form. Based on the compression algorithm and parameters used, the data was reversed to return to its original state. Data compression includes lossless compression and lossy compression. The experiment adopts lossless compression method. Common lossless compression algorithms include Huffman encoding, Lempel Ziv Welch encoding,

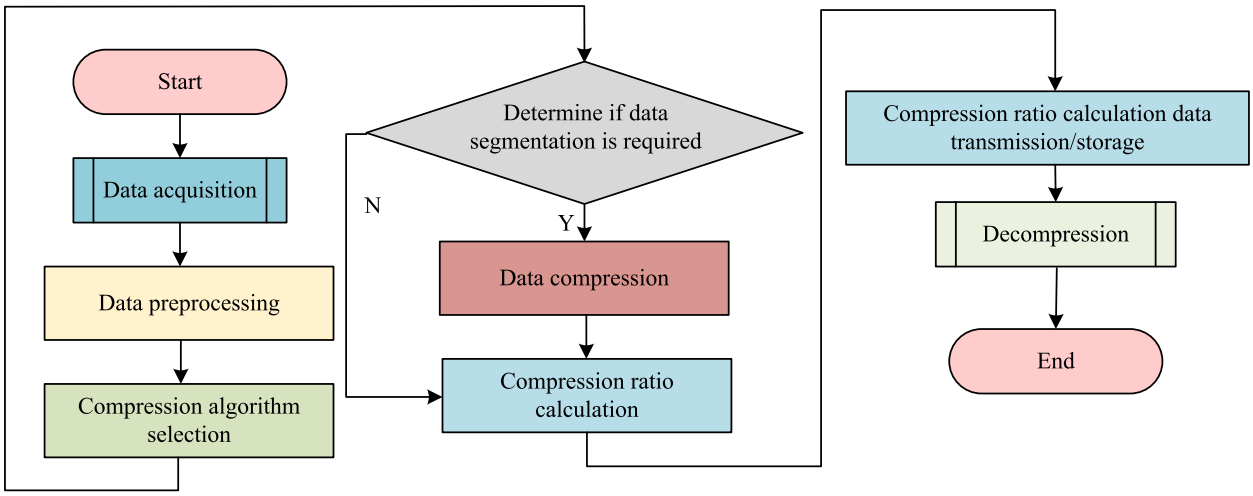

FIGURE 5. Different intelligent terminal data compression processes.

and Burrows Wheeler Transform [23]. Lexicon Ziv Welch achieves data compression by establishing a dictionary and encoding consecutive character sequences. Equation (1) is a function of data sequence length.

$$\eta(x) = \frac{x}{h}\lg x - \frac{Ax}{h} - \frac{xl}{k} + (\frac{\lg x}{h}) \tag{1}$$

In Equation (1), x represents the number of codewords generated during data compression, which is information entropy.When compressing a data sequence with a length of n compression, and when n approaches infinity, the asymptotic solution in Equation (2) can be obtained from Equation (1).

$$x_n = \frac{nh}{\lg n}(1 + \frac{\lg\lg n}{\lg n} + \frac{A - \lg h}{\lg n} + O(\frac{(\lg\lg n)^2}{\lg^2 n})) \tag{2}$$

In Equation (2), x_n represents the number of codewords generated by compression. Burrows Wheeler Transform sorts the circular rotation of strings to obtain a new string and extracts the last column from the original string. This new string can be better compressed in some cases, as it will result in blocks with consecutive occurrences of the same character. For the data of a $M \times N$ matrix, assume that the vector originally composed of the first column of M is $R = acdeee$ and the last column of the matrix is C. The experiment moved C to the forefront to form a new matrix in Equation (3).

$$M_{new}(i, j) = M(i, (j-1) \bmod (N)) \tag{3}$$

In Equation (3), i represents the i-th row of matrix. j represents the j-th column. Each element in $T(j)$ represents the number of rows in M corresponding to the j-th row of M_{new} in Equation (4).

$$F(T(j)) = C(j) \tag{4}$$

In Equation (4), T represents a transformation vector. In Equation (5), the original vector S can be obtained by recursion.

$$S(N-1-i) = L(T^i(I)) \tag{5}$$

In Equation (5), $i = 1, 2, \ldots, N-1$, $T^0(x) = x$. Huffman encoding constructs a variable length encoding table to represent characters with higher frequencies with shorter encodings, while characters with lower frequencies are represented with longer encodings. This encoding method can effectively reduce storage space, especially suitable for data such as text that contains more repetitive characters. Huffman encoding does not require the establishment of a dictionary or sorting of data in advance, making it suitable for dynamic or real-time data in Figure 6.

For the data to be encoded, it is first necessary to calculate the frequency of each character's occurrence. Then, a Huffman tree was constructed based on character frequency. Each character is treated as a leaf node and a tree is constructed based on frequency. Characters with lower frequencies are located in the lower part of tree, while characters with higher frequencies are located in the higher part of tree. Further allocation encoding was carried out, starting from the root node, marking the left path as 0 and the right path as 1. Each character was assigned a unique binary encoding along Huffman tree. Upon reaching each leaf node, Huffman encoding for each character is obtained. Finally, by establishing a mapping relationship between each character and its corresponding Huffman encoding representation, an encoding table is formed. Equation (6) is the weighted path length oftree.

$$WPL = \sum_{i=1}^{n} w_i l_i \tag{6}$$

In Equation (6), n represents the number of nodes. l_i represents the path length from the root node to leaf node. w_i represents the weight value of each leaf node. Huffman number is also known as the optimal binary tree. Data encryption is important in protecting privacy, preventing data tampering, resisting network attacks, and complying with regulatory requirements. By encrypting, data security can be effectively improved and the risk of data leakage and damage can be

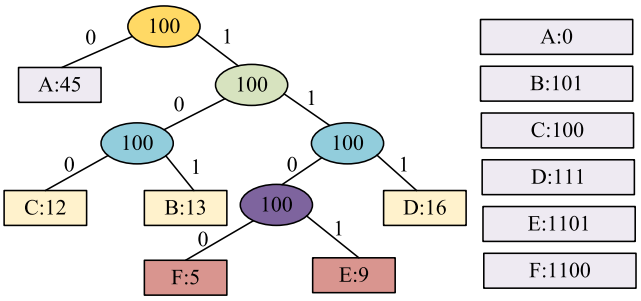

FIGURE 6. Schematic diagram of Huffman encoding.

reduced. By combining Huffman encoding and HEVCDCT data encryption, the confidentiality of video content can be protected, content leakage can be prevented, data security can be improved, and the ability to resist attacks during video transmission and storage can be enhanced. This is crucial for ensuring the security and confidentiality of video content, especially in scenarios involving sensitive information. HEVC aims to provide higher compression efficiency, which means using lower bit rates to transmit or store video data under the same visual quality. This means that HEVC can achieve higher quality video transmission while reducing bandwidth requirements and storage costs in Figure 7.

In HEVC, the main modules collaborate with each other to achieve the goals of high compression efficiency and high-quality visual quality. Firstly, as the starting point of HEVC, the encoder carries the important task of receiving raw video data and initiating the entire compression process. Next, the transformation and quantization module performs a series of precise operations on the input video data, converting pixel data from spatial domain to frequency domain through transformation, and then simplifying frequency domain data through quantization to effectively reduce data volume. Although these two processes introduce a certain degree of data loss, after optimization, their impact on visual quality can be negligible. At the decoding end, the inverse quantization and inverse transformation modules bear the heavy responsibility of reconstructing the original video. Through inverse quantization and inverse transformation operations, data is accurately restored from the frequency domain back to the spatial domain, providing an accurate foundation for subsequent reconstruction processes. In order to further improve compression efficiency, the filtering data module plays a crucial role. It utilizes advanced filtering technology to effectively remove redundancy in data, and further optimizes data representation through operations such as prediction, denoising, and smoothing. Entropy encoding, as the final stage of the compression process, efficiently encodes data based on its statistical characteristics, assigning shorter codewords to the data generated in the previous steps, thereby achieving lossless compression and ensuring data integrity and accuracy. At the same time, the motion data module delves into the redundant information between video frames. By accurately analyzing key information such as motion vectors, this module effectively improves the efficiency of prediction encoding, enabling HEVC to fully utilize the inherent characteristics of videos. Finally, the fusion module cleverly integrates various coding strategies and tools together, ensuring that all parts work together and complement each other to achieve the highest compression efficiency.In HEVC, DCT decomposes the input signal into cosine function components of different frequencies and represents the amplitude of each component. By using cosine functions of different sizes and directions, DCT decomposes the signal into a series of frequency components. These frequency components have higher frequencies at higher positions. Equation (7) is the mathematical definition of DCT.

$$f(x,y) = \sum_{p=0}^{M-1}\sum_{q=0}^{N-1} c(p)c(q)u(x,y) \tag{7}$$

In Equation (7), $p = 0, 1, \ldots M-1$, $q = 0, 1, \ldots N-1$. Assuming DCT image is a matrix of $N \times N$, DCT in Equation (8) can be obtained.

$$F(u,v) = \sum_{i=0}^{M-1}\sum_{j=0}^{N-1} c(u)c(v)f(i,j)\cos\left[\frac{(i+0.5\pi)}{N}u\right] \times \cos\left[\frac{(i+0.5\pi)}{N}v\right] \tag{8}$$

In Equation (8), $c(u)$ and $c(v)$ represent the coefficients used for normalization, respectively. Equation (9) represents $c(u)$.

$$c(u) = \begin{cases} \sqrt{\frac{1}{N}}, u = 0 \\ \sqrt{\frac{2}{N}}, u \neq 0 \end{cases} \tag{9}$$

In Equation (9), N is the size of the input signal. $F(0,0)$ is usually referred to as directcurrent coefficient, while the values at other positions are referred to as alternating current (AC) coefficient. When encrypting, DCT coefficient block and AC coefficient are first perturbed, and then directcurrent coefficient is encrypted using XOR encryption in Figure 8.

DCT used in data compression divides images or videos into small blocks and obtains directcurrent and AC coefficients through the quantization process. There is a correlation between these coefficients, and there is also a certain degree of data correlation between AC coefficients. This correlation may be exploited by interceptors to obtain the content of the transmitted data. In order to increase the security of data encryption transmission, data can be subjected to disturbance processing. At this stage, XOR encryption can be used to reduce additional memory space consumption. Specifically, DCT data block perturbation function can be used to generate binary sequences of random numbers as reference data for XOR encryption. To ensure proper processing, the length of the random number sequence should be consistent with the binary sequence length of directcurrentcoefficient. If the length is inconsistent, 0 needs to be filled in at the beginning of sequence. By perturbing and XOR encrypting data, it can

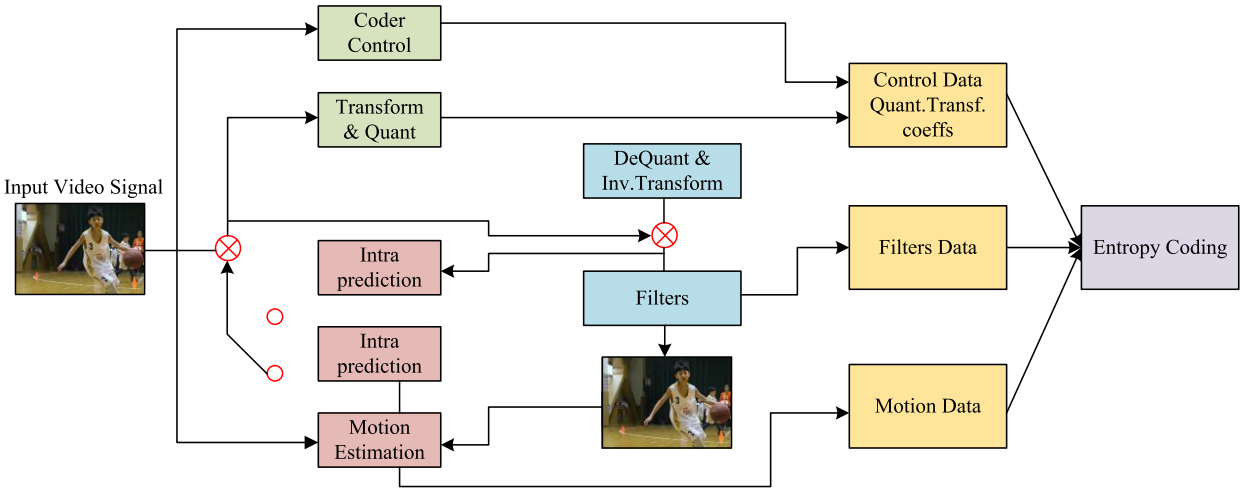

FIGURE 7. HEVC schematic diagram.

increase the difficulty for interceptors to interpret data content, provide additional layers of protection, and ensure the security of encrypted data transmission. Equation (10) is a binary sequence of directcurrent coefficients.

$$S_{DC} = s_1 s_2 s_3 \ldots s_n \tag{10}$$

In Equation (10), $s_i \in 0, 1$. Equation (11) is a binary sequence of random numbers.

$$S_{key} = k_1 k_2 k_3 \ldots k_n \tag{11}$$

In Equation (11), $k_i \in 0, 1$. Equation (12) represents the sequence of ciphertext generated by directcurrentcoefficients after XOR encryption.

$$S_e = e_1 e_2 e_3 \ldots e_n \tag{12}$$

In Equation (12), $e_i \in 0, 1$. Equations (10), (11), and (12) need to satisfy a certain XOR relationship in Equation (13).

$$e_i = s_i \oplus k_i \tag{13}$$

In Equation (13), $i = 1, 2, \ldots n$. The study adopts IEEE 1451 as the communication standard, which is used for communication and interoperability between sensors and measurement devices. A universal sensor and measurement device architecture has been defined, including physical layer, data format, network protocol, and software interface. EEE 1451 protocol family consists of multiple standards, including the following core standards. IEEE 1451.0 defines the framework and concepts of the entire protocol family. IEEE 1451.1 defines the network communication interfaces for sensors and measurement devices. IEEE 1451.2 defines the data formats and encoding methods for sensors and measuring equipment. IEEE 1451.3 defines wireless communication interfaces for sensors and measurement devices. IEEE 1451.4 defines device descriptions and discovery mechanisms for sensors and measuring devices. IEEE 1451.5 defines self diagnosis and calibration mechanisms for sensors and measuring equipment. These standards collectively provide consistent interfaces and communication protocols for sensors and measurement devices to achieve device interoperability and ease of integration.

IV. ANALYSIS OF THE APPLICATION EFFECT OF UNIFIED ACCESS TECHNOLOGY FOR INTELLIGENT DEVICES AND DC TECHNOLOGY

This chapter includes two sub sections. Firstly, comparative experiments were conducted on three encoding methods: Huffman encoding, Sprite encoding, and dictionary encoding.Then, the optimization effect of JHC-DCT model was analyzed. The second section analyzes the application effect and performance of MIC-IoTAS model, as well as the power consumption of FPGA components.

A. PERFORMANCE ANALYSIS OF JHC-DCT ALGORITHM

This experiment first compares three coding methods: Hoffman coding, Sprite coding and dictionary coding. And BWT (Burrows-Wheeler Transform, BWT) were introduced as comparison.The purpose is to evaluate their performance and effectiveness in different scenarios to determine their most suitable application scenario. Various measures and methods to evaluate the performance and accuracy of the proposed scheme. It mainly includes transmission efficiency and coding time. Transmission efficiency measures the amount of data that the system can transmit in unit time. Transmission efficiency is obtained by calculating the ratio of the amount of data transmitted to the transmission time. Cocoding time represents the time required for the system to encode data. In this paper, the efficiency of the new scheme is measured by comparing the coding time required by the traditional Hoffman coding technique with the proposed technique. To measure the above metrics, the article performs experimental testing. In the experiment, the researchers used different smart devices and transmitted the data through the proposed scheme. During the course of the experiment, the

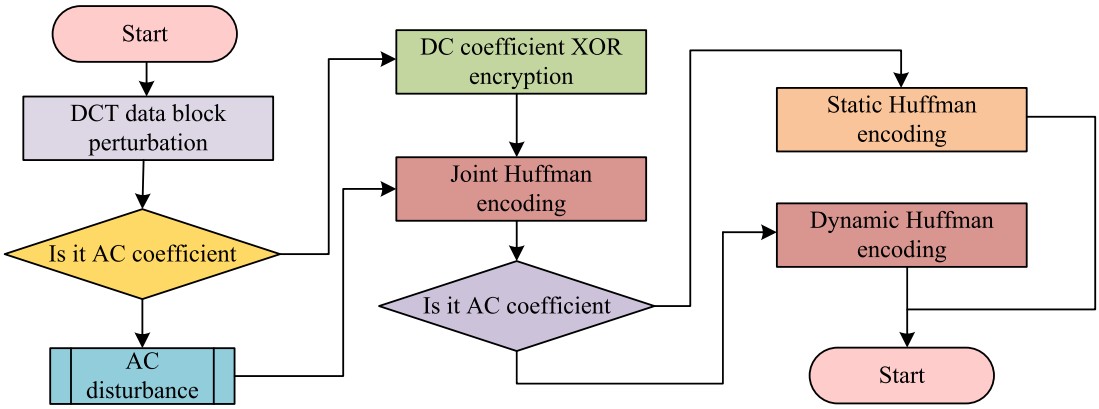

FIGURE 8. HEVC encryption process with joint Huffman encoding.

researchers recorded the transmitted data quantity, transmission time and coding time, and analyzed these data to get the specific value of transmission efficiency and coding time. The importance of transmission efficiency is that it directly reflects the data transmission capability of the scheme. A high transmission efficiency means that the system can transmit more data per unit of time, which is particularly important for real-time applications and big data transmission scenarios [24]. The importance of encoding time is that it affects the response time of the system. The shorter encoding time means that the system can process the data faster, which is important for application scenarios requiring rapid response.This experiment prepared 300MB of ASCII text, HTML files, log file format text data, as well as 300MB of JPEG, PNG, BMP format image data, as well as 300MB of AVI, MP4, and MKV format video data, with compression rate as the evaluation indicator in Figure 9.

Figure 9 shows the compression rate of various data formats after applying three different compression methods. From Figure 9, all three methods perform well in compressing text type data, with compression rates above 50%. In addition, when sprite encoding and dictionary encoding compress data in both image and video formats, the compression efficiency is relatively low. The compression efficiency of Huffman encoding for AVI, MP4, and MKV is 60.5%, 63.4%, and 60.6%, respectively, which is more than 10% higher than sprite encoding and more than 30% higher than dictionary encoding. When using dictionary encoding to compress video data, the compression rate does not exceed 30%. When using Huffman encoding to compress various data types, the compression rate is relatively high, all exceeding 60%, indicating that this encoding method can more effectively reduce the storage space of data when compressing videos.However, the BWT coding method generally performed well, but it is still inferior to the Hoffman coding adopted in the study.To study the optimization effect of JHC-DCT model, the experiment used the model to transmit 10G video data, with transmission rate V and efficiency B as the average indicators in Figure 10.

Figure 10 shows the transmission efficiency of JHC-DCT model and its variation over time during the experimental

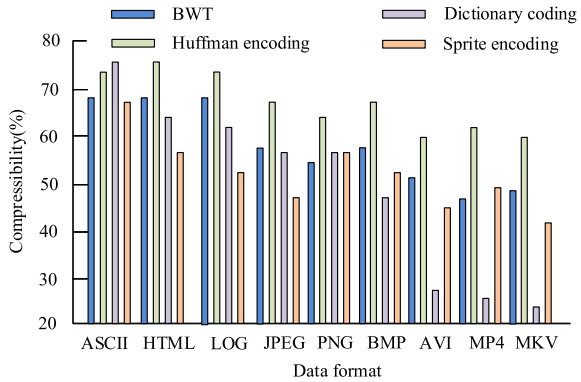

FIGURE 9. Compression rate of each data format.

process. According to Figure 10 (a), the transmission rate of the model fluctuates between 8MB and 14MB per second. This means that the transmission rate has some fluctuation, but overall the propagation rate is relatively high. According to Figure 10 (b), the propagation efficiency of JHC-DCT coefficient model ranges from 67% to 87%, with an average of approximately 73%. This indicates that the actual proportion of effective information carried during transmission is relatively high. These results confirm that the model can effectively retain and transmit important information content when transmitting data. These results provide information on the performance of the model when transmitting data, and provide a reference basis for further optimizing and improving the transmission efficiency of the model. To further evaluate the performance of JHC-DCT model, PSNR and SSIM indicator systems were introduced in the experiment. PSNR is a measure of the difference between the original image and the compressed or processed image. It calculates by comparing the mean square error between the pixel values of the original image and the processed image. SSIM is a structural similarity indicator that measures the degree of perceptual similarity between two images. SSIM uses brightness, contrast, and structure to compare the differences between images. It takes into account the sensitivity of the human eye to brightness and texture structure, thus more in line

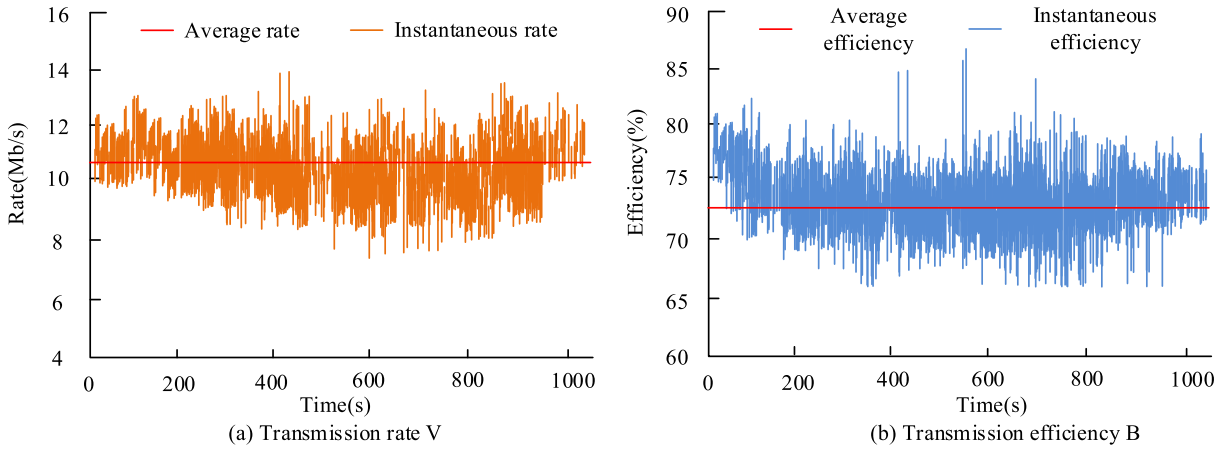

FIGURE 10. Changes in transmission efficiency of JHC-DCT model.

with the characteristics of human perception of image quality. The range of SSIM values is 0 to 1, and Figure 11 is the experimental results.

Figure Figure 11 shows the comparison to SSIM of PSNR values for the JHC-DCT model. Where the I frame is usually periodically inserted as a reference point, and the P and B frames are used to describe the differences between adjacent frames. The selection and combination of such frame types contribute to the high efficiency and reliability of video compression and transmission. The D frame contains only information about DC (DC) components, no motion vector or AC (AC) components. It is evident from Figure 11 (a) that the JHC-DCT model performs well in the PSNR with higher values than the Huffman-encoded PSNR. This means that the images compressed and transmitted by JHC-DCT have less difference between the original images after reconstruction and thus higher image quality. In particular, JHC-DCT has 4.4 more P frames than Huffman coding, a significant boost attributed to the more efficient compression strategy of the JHC-DCT model and the ability to accurately describe inter-frame differences. Figure 11 (b) shows the comparison in terms of SSIM values. Impressively, the SSIM of the JHC-DCT model is more than 15% higher than the Huffman-coded SSIM. This obvious advantage further validates the superiority of the JHC-DCT model in video compression and transmission. Especially for the I frames of the JHC-DCT, which are 22 percent higher than the Huffman codes, which strongly illustrates the superior performance of the JHC-DCT model when handling critical reference frames. In conclusion, the excellent performance of the JHC-DCT model on two key indicators, PSNR and SSIM, fully demonstrates its advantages in the field of video compression and transmission. This advantage stems from its fine frame type selection strategy, as well as its efficient compression algorithm design. Therefore, the JHC-DCT model is expected to become the mainstream technology in the field of video compression and transmission in the future, meeting the growing demand for HD and uHD video transmission. The

TABLE 1. JHC-DCT and Huffman encoding time.

Video Number	Encoding time consumption(ms)	Huffman encoding takes time(ms)	Time difference(ms)	Time consumption decrease rate(%)
V16548	160081	185811	25730	13.84
V16457	69894	78531	8637	10.99
V16897	98726	120568	21842	18.12
V16879	184081	208465	24384	11.69
V16896	168981	186542	17561	9.41
V16549	68419	86541	18122	20.94

experiment also recorded the time-consuming situation of the JHC-DCT model with the Huffman encoding, and the results are shown in Table 1.

Table 1 shows the comparison of encoding time between the two models. In coding, JHC-DCT model has higher efficiency compared to Huffman coding. Specifically, JHC-DCT model can reduce encoding time by approximately 10%, with a maximum reduction of 20.94% and a minimum reduction of 9.41% in the tested samples. Therefore, by using JHC-DCT model, the encoding time was significantly reduced.

B. ANALYSIS OF THE APPLICATION EFFECT AND PERFORMANCE OF MIC-IOTAS MODEL

To analyze the application effect of MIC-IoTAS, a comparative analysis was conducted on the usage of various resources in Figure 12. They include FF triggers for composing sequential logic circuits, LUT lookup tables for implementing various combinatorial and sequential logic, block memory BRAM for creating large capacity, fast storage arrays and FIFOs, global buffers belonging to global clock resources, and IO.

Figure 12 shows the usage of different resource types in MIC-IoTAS and IoTAS strategies. When comparing MIC-IoTAS and IoTAS schemes, FF trigger utilization rate of MIC-IoTAS scheme is about 5%, which is 1% lower than the IoTAS scheme. In addition, in MIC-IoTASFF scheme, the utilization rate of LUT lookup tables is approximately 6,

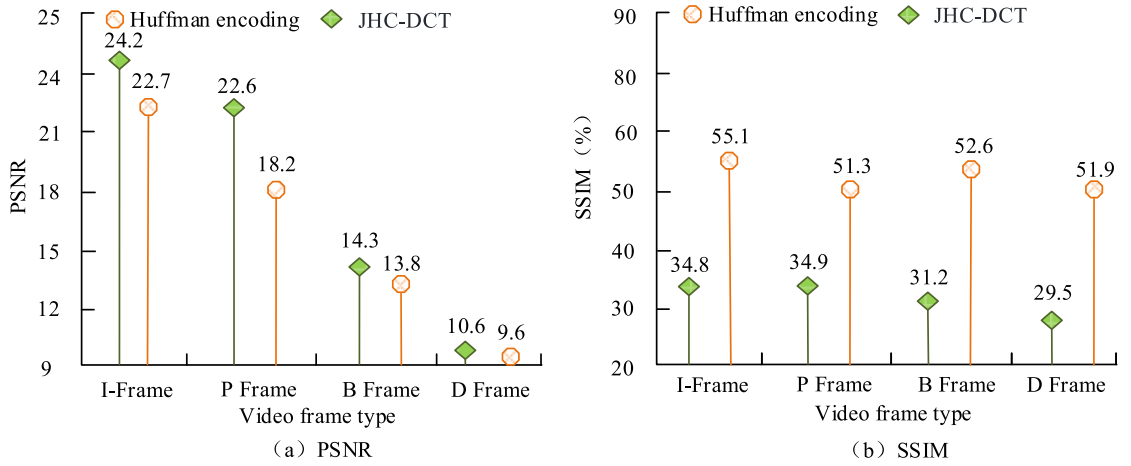

FIGURE 11. Comparison between PSNR value and SSIM value.

which is an increase compared to the IoTAS scheme. In addition, the I/O utilization rate in MIC-IoTASFF scheme is about 4%, which is 6% lower than the IoTAS scheme. Similarly, the utilization rate of BUFG (clock buffer) in MIC-IoTASFF scheme is 9%, which is 2% lower than the IoTAS scheme. Finally, the utilization rate of BRAM (block RAM) in MIC-IoTASFF scheme was 22%, a decrease of 11% compared to the IoTAS scheme. Based on the above data comparison, MIC-IoTASFF scheme differs in the usage of different components compared to the IoTAS scheme. The usage rates of LUT, I/O, BUFG, and BRAM have all improved or decreased, and the overall resource utilization rate is at a low level, saving a lot of resources. To test the practical application effect of MIC-IoTAS, a strategy was adopted to build a smart office using digital cameras, sensors, and other related terminals. All these terminals are uniformly connected through MIC-IoTAS and interconnected with the system. In this way, the functionality and performance of MIC-IoTAS in an intelligent office environment can be fully evaluated. In this way, the reliability, security, and compatibility with various TDs of MIC-IoTAS in practical scenarios can be tested. The construction of this smart office will provide important feedback information. Figure 13 shows the layout of various terminals.

Figure 13 shows the layout of various TD systems in a smart office based on MIC-IoTAS. This includes video surveillance systems, intelligent lighting systems, sensor networks, and intelligent power management systems. Through cameras and network connections, the video surveillance system achieves monitoring and recording functions for the interior and surrounding areas of the office, as well as improving security. Intelligent lighting systems can improve energy efficiency and comfort by automatically adjusting lighting brightness and color temperature through sensors or preset plans. Sensor networks, including temperature sensors, humidity sensors, light sensors, etc., are used to monitor environmental data and automatically adjust office settings. Through intelligent sockets and energy monitoring devices,

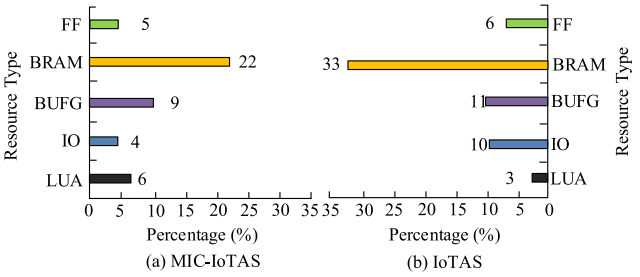

FIGURE 12. Usage of different resource types.

the intelligent power management system achieves control and optimization of power consumption, improving energy efficiency. After two months of system testing, a large amount of data were collected and monitored in real-time through mobile or PC terminals. Figure 14 shows the 60 day average.

Figure 14 shows the temperature and PM2.5 changes in the command office during various time periods within 60 days. According to Figure 14 (a), the temperature inside the smart office fluctuates between 8 and 21 degrees Celsius. This temperature fluctuation may be due to the automatic adjustment function of the air conditioning system used in the room to maintain a comfortable working environment. The reason for relatively small temperature fluctuations during the day may be due to factors such as personnel activity, equipment operation, and relatively stable external temperatures. According to Figure 14 (b), PM2.5 concentration in the smart office fluctuates between 360 and 790. The concentration changes within this range may be caused by a combination of factors such as indoor and outdoor air flow, personnel activities, harmful substances released from indoor decoration materials, and outdoor environmental pollution. It is particularly noteworthy that during the 0-15 period, PM2.5 concentration remains relatively stable. This may be because during this period, the ventilation system in the office operated normally, there was less personnel activity, or other control measures were taken, which helped to maintain low

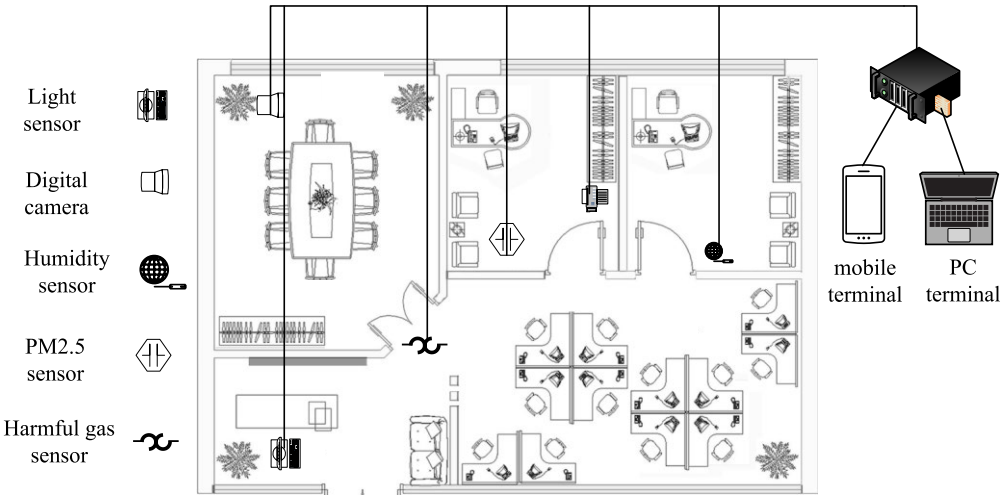

FIGURE 13. Smart office layout plan.

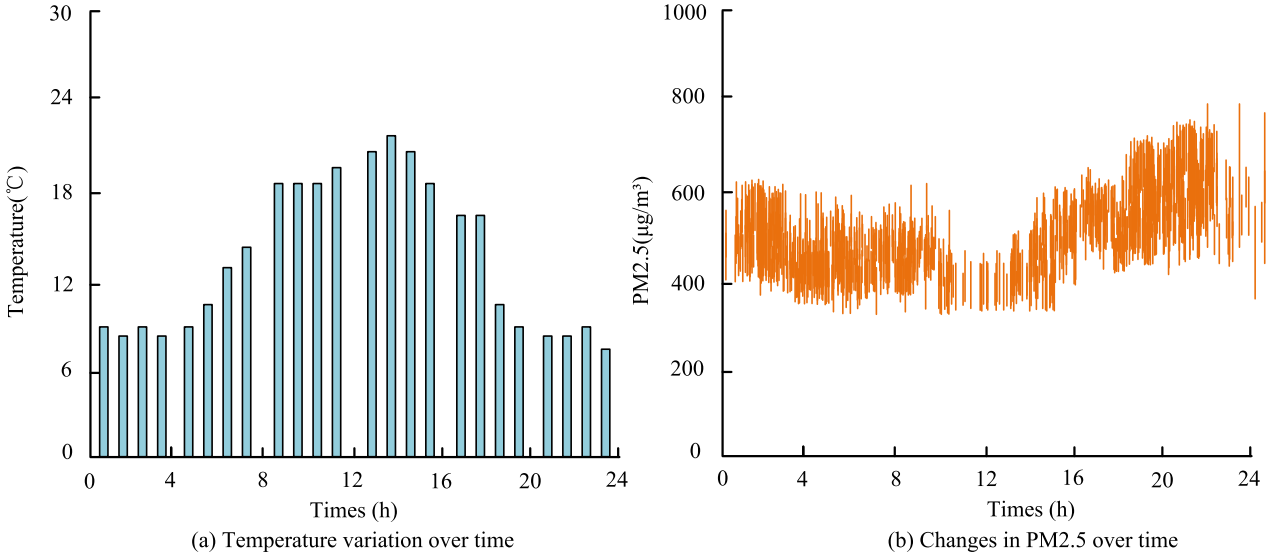

(a) Temperature variation over time (b) Changes in PM2.5 over time

FIGURE 14. Changes in temperature and PM2.5 over a period of 60 days.

PM2.5 levels. However, starting from 15:00, the concentration of PM2.5 gradually increased, possibly due to increased afternoon activities, weakened ventilation effects, or other pollution sources. The experiment also recorded the power consumption of the FPGA in Figure 15.

Figure 15 reveals the power consumption details of the numerous components in the FPGA. From an overall perspective, the total power consumption of the entire FPGA system is about 1.74 watts, indicating its energy consumption during the working process. From the perspective of power consumption, the static power consumption is about 0.16 watts, accounting for 9% of the total power consumption of the system, while the dynamic power consumption accounts for a larger proportion, at about 1.58 watts, accounting for 91% of the total power consumption of the system. This means that the dynamic power consumption is the main source of the power consumption in the FPGA system. Further study of the dynamic power consumption can find the specific contribution of each component to the power consumption. The power consumption of the clock is 0.007 watts, the signal power consumption is 0.003 watts, and the local power consumption is 0.002 watts. In addition, the power consumption of BRRAM (block RAM) is 0.007 watts, which is comparable to other components. The input and output (IO) power consumption and XADC (analog-to-digital converter) have the lowest power consumption of 0.001 watts. It is worth mentioning that the PS7 (programmable system integrated circuit processing system) power consumption is significantly high, reaching 1.567 watts, accounting for the vast majority of the dynamic power consumption. This difference indicates the more power support required for PS7 when performing complex tasks. In conclusion, the various components of the FPGA differ in their power consumption. The PS7 is the most power-consuming component because it contains

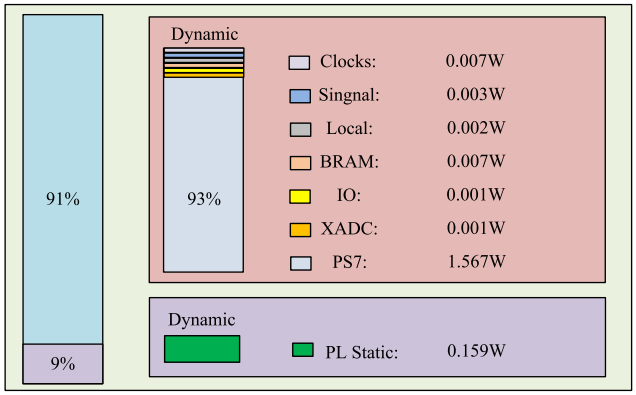

FIGURE 15. Power consumption of various components in the FPGA system.

high-performance processors and associated functional modules. While relatively low power consumption components such as IO and XADC are usually responsible for simple input/output interfaces and analog-to-digital conversion operations, thus having low power consumption. This difference in power consumption reflects the imbalance in the functional complexity and energy requirements of the different components within the FPGA.

V. CONCLUSION

This study aims to explore and study the performance of diversified td devices to provide new solutions for efficient data communication of terminal devices and seamless interconnection of terminal devices.JHC-DCT network communication scheme and MIC-IoTAS terminal access scheme were established. The experiment first conducted a comparative experiment on three encoding methods: Huffman encoding, sprite encoding, and dictionary encoding. These results confirm that sprite encoding and dictionary encoding have lower compression efficiency when compressing data in both image and video formats. Especially when using dictionary encoding to compress video data, the compression rate does not exceed 30%. When using Huffman encoding to compress various data types, the compression rate is relatively high, all exceeding 60%, indicating that this encoding method can more effectively reduce the storage space of data when compressing videos. To study the optimization effect of JHC-DCT model, the experiment utilized the model to transmit 10G video data. These results confirm that PSNR of JHC-DCT model is higher than Huffman encoded PSNR, indicating that the smaller the difference between the compressed and transmitted images through JHC-DCT, the better the image quality. Moreover, the SSIM of JHC-DCT model is more than 15% lower than Huffman encoded SSIM, which proves the superiority of this model. In addition, the experiment validated the use of MIC-IoTAS and IoTAS strategies for different resource types. These results confirm that FF trigger usage rate of MIC-IoTAS is approximately 5%, which is 1% lower thanIoTAS. The IO usage rate in MMIC-IoTASFF scheme is 4%, which is 6% lower than IoTAS. The usage rate of BUFG in MIC-IoTASFF scheme is 9%, which is 2% lower than that of IoTAS. The usage rate of BRAM in MIC-IoTASFF scheme is 22%, which is 11% lower than that of IoTAS. By comparing the above data, it is not difficult to find that the overall resource utilization rate of MIC-IoTASFF proposed in the study is at a low level, saving a lot of resources. However, the utilization rate of LUT lookup tables in IC-IoTASFF scheme is about 6%, which is 3% higher than IoTAS. This is also an aspect that needs improvement in future research.

REFERENCES

[1] M. U. Danjuma, B. Yusuf, and I. Yusuf, "Reliability, availability, maintainability, and dependability analysis of cold standby series-parallel system," *J. Comput. Cognit. Eng.*, vol. 1, no. 4, pp. 193–200, Jul. 2022, doi: 10.47852/bonviewJCCE2202144.

[2] N. Shakeel, P. Teradata, and S. Shakeel, "Context-free word importance scores for attacking neural networks," *J. Comput. Cognit. Eng.*, vol. 1, no. 4, pp. 187–192, Sep. 2022, doi: 10.47852/bonviewJCCE2202406.

[3] P. A. Ejegwa and J. M. Agbetayo, "Similarity-distance decision-making technique and its applications via intuitionistic fuzzy pairs," *J. Comput. Cognit. Eng.*, vol. 2, no. 1, pp. 68–74, Feb. 2022, doi: 10.47852/bonviewJCCE512522514.

[4] Z. Li, Y. Dong, L. Fu, J. Zhao, J. Li, and W. Zheng, "Integrated research on power distribution intelligent switching equipment," *Int. Core J. Eng.*, vol. 6, no. 1, pp. 48–54, May 2020.

[5] J. Reidy, C. Brown-Johnson, N. McCool, S. Steadman, M. B. Heffernan, and V. Nagpal, "Provider perceptions of a humanizing intervention for health care workers—A survey study of PPE portraits," *J. Pain Symptom Manage.*, vol. 60, no. 5, pp. e7–e10, Nov. 2020.

[6] A. Ren, H. Wang, W. Zhang, J. Wu, Z. Wang, R. V. Penty, and I. H. White, "Emerging light-emitting diodes for next-generation data communications," *Nature Electron.*, vol. 4, no. 8, pp. 559–572, Aug. 2021, doi: 10.1038/s41928-021-00624-7.

[7] G. Aceto, V. Persico, and A. Pescapé, "A survey on information and communication technologies for Industry 4.0: State-of-the-art, taxonomies, perspectives, and challenges," *IEEE Commun. Surveys Tuts.*, vol. 21, no. 4, pp. 3467–3501, 4th Quart., 2019, doi: 10.1109/COMST.2019.2938259.

[8] C. V. Poulton, M. J. Byrd, P. Russo, E. Timurdogan, M. Khandaker, D. Vermeulen, and M. R. Watts, "Long-range LiDAR and free-space data communication with high-performance optical phased arrays," *IEEE J. Sel. Topics Quantum Electron.*, vol. 25, no. 5, pp. 1–8, Sep. 2019, doi: 10.1109/JSTQE.2019.2908555.

[9] X. Wang, X. Chen, and X. Wang, "Secure vehicular data communication in named data networking," *Digit. Commun. Netw.*, vol. 9, no. 1, pp. 203–210, Feb. 2023.

[10] J. Sekera and A. Novák, "The future of data communication in Aviation 4.0 environment," *INCAS Bull.*, vol. 13, no. 3, pp. 165–178, Sep. 2021, doi: 10.13111/2066-8201.2021.13.3.14.

[11] N. J. Kholit and M. Nastain, "Mapping of data communication networks on social media," *Interdiscipl. J. Commun.*, vol. 5, no. 2, pp. 143–162, Jan. 2021, doi: 10.18326/inject.v5i2.143-162.

[12] A. Modares, M. Kazemi, V. B. Emroozi, and P. Roozkhosh, "A new supply chain design to solve supplier selection based on Internet of Things and delivery reliability," *J. Ind. Manage. Optim.*, vol. 19, no. 11, pp. 7993–8028, Jul. 2023, doi: 10.3934/jimo.2023028.

[13] S. Kumar, P. Tiwari, and M. Zymbler, "Internet of Things is a revolutionary approach for future technology enhancement: A review," *J. Big Data*, vol. 6, no. 1, pp. 1–21, Dec. 2019, doi: 10.1186/s40537-019-0268-2.

[14] N. Alsharari, "Integrating blockchain technology with Internet of Things to efficiency," *Int. J. Technol., Innov. Manage.*, vol. 1, no. 2, pp. 1–13, Dec. 2021, doi: 10.54489/ijtim.v1i2.25.

[15] R. P. Singh, M. Javaid, A. Haleem, and R. Suman, "Internet of Things (IoT) applications to fight against COVID-19 pandemic," *Diabetes Metabolic Syndrome, Clin. Res. Rev.*, vol. 14, no. 4, pp. 521–524, Jul. 2020, doi: 10.1016/j.dsx.2020.04.041.

[16] Y. Liu, J. Wang, J. Li, S. Niu, and H. Song, "Machine learning for the detection and identification of Internet of Things devices: A survey," *IEEE Internet Things J.*, vol. 9, no. 1, pp. 298–320, Jan. 2022, doi: 10.1109/JIOT.2021.3099028.

[17] H. Xie and Z. Qin, "A lite distributed semantic communication system for Internet of Things," *IEEE J. Sel. Areas Commun.*, vol. 39, no. 1, pp. 142–153, Jan. 2021, doi: 10.1109/JSAC.2020.3036968.
[18] S. Mittal, "A survey of FPGA-based accelerators for convolutional neural networks," *Neural Comput. Appl.*, vol. 32, no. 4, pp. 1109–1139, Feb. 2020, doi: 10.1007/s00521-018-3761-1.
[19] J. Zhang and G. Qu, "Recent attacks and defenses on FPGA-based systems," *ACM Trans. Reconfigurable Technol. Syst.*, vol. 12, no. 3, pp. 1–24, Aug. 2019, doi: 10.1145/3340557.
[20] Y. Yu, C. Wu, T. Zhao, K. Wang, and L. He, "OPU: An FPGA-based overlay processor for convolutional neural networks," *IEEE Trans. Very Large Scale Integr. (VLSI) Syst.*, vol. 28, no. 1, pp. 35–47, Jan. 2020, doi: 10.1109/TVLSI.2019.2939726.
[21] L. Zhang, F. Li, and C. Qin, "Efficient reversible data hiding in encrypted binary image with Huffman encoding and weight prediction," *Multimedia Tools Appl.*, vol. 81, no. 20, pp. 29347–29365, Apr. 2022, doi: 10.1007/s11042-022-12710-9.
[22] P. A. van Walree and M. E. G. D. Colin, "In situ performance prediction of a coherent acoustic modem in a reverberant environment," *IEEE J. Ocean. Eng.*, vol. 47, no. 1, pp. 236–254, Jan. 2022, doi: 10.1109/JOE.2021.3085942.
[23] W. Liang, D. Zhang, X. Lei, M. Tang, K.-C. Li, and A. Y. Zomaya, "Circuit copyright blockchain: Blockchain-based homomorphic encryption for IP circuit protection," *IEEE Trans. Emerg. Topics Comput.*, vol. 9, no. 3, pp. 1410–1420, Jul. 2021.
[24] A. S. Panayides, A. Amini, N. D. Filipovic, A. Sharma, S. A. Tsaftaris, A. Young, D. Foran, N. Do, S. Golemati, T. Kurc, K. Huang, K. S. Nikita, B. P. Veasey, M. Zervakis, J. H. Saltz, and C. S. Pattichis, "AI in medical imaging informatics: Current challenges and future directions," *IEEE J. Biomed. Health Informat.*, vol. 24, no. 7, pp. 1837–1857, Jul. 2020, doi: 10.1109/JBHI.2020.2991043.

XUEYAN WANG was born in Taizhou, Zhejiang, China, in December 1994. She received the master's degree in electrical engineering from Hunan University, in June 2020.

From September 2020 to present, she is an employee of the Production and Research Department of the Technology Branch of State Grid Zhejiang Electric Power Supply Company, Taizhou Branch, Taizhou Hongchuang Power Group Company Ltd. She was a technology project leader for five times. She has applied for over 50 invention patents, authorized over 20 invention patents, published four high-level journal articles, and completed two enterprise level gold medal product releases.

HONGLIANG ZOU was born in Gao'an, Jiangxi, China, in June 1982. He received the bachelor's degree in electronic information engineering, the master's degree in power electronics and power transmission, and the Ph.D. degree in power system and automation from Wuhan University, in 2004, 2007, and 2017, respectively.

He has expertise in new power systems and artificial intelligence. From 2012 to 2017, he was a specialist in the maintenance and repair of switches, transformers, and substations in the Operation and Maintenance Department. From 2017 to 2020, he was the Deputy Director of the Operations and Maintenance Department (in charge of power transformation and planning). From 2020 to 2021, he was the Deputy Director of the Internet Office. Since 2021, he is the Manager of State Grid Zhejiang Electric Power Supply Company, Taizhou Branch and Hongchuang Group Technology Branch, he awarded a total of four invention patents in the fields of artificial intelligence and power energy, and have published six papers in the field of power technology, including three papers in IE conferences, one paper in electrical technology, and two papers in high-voltage technology.

HAIBO LI was born in Taizhou, Zhejiang, China, in May 1983. He received the bachelor's degree in automation and the master's degree in electrical engineering, with a research direction in power systems and automation from Chongqing University, in 2005 and 2010, respectively.

From 2010 to 2013, he was a full-time Employee with the Transmission and Inspection Center, State Grid Taizhou Power Supply Company, where he was also a full-time Employee with the Human Resources Department, from 2014 to 2018. From 2018 to 2021, he was the Deputy Director of the Transmission and Inspection Center, State Grid Taizhou Power Supply Company. From 2023 to present, he worked as the Party Branch Secretary and Deputy Manager of the State Grid Zhejiang Electric Power Supply Company, Taizhou Branch, Hongchuang Power Group Company Ltd. He was a leader of a technology project (twice), applied for two invention patents, published four Chinese core and EI papers on the project, and studied new power systems and artificial intelligence.

HEMING QIAN was born in Taizhou, Zhejiang, in November 1996. He received the bachelor's degree in electrical engineering and automation from the Northwest University for Nationalities, in 2019.

From 2019 to 2022, he was a member of the Jiaobei Power Supply Station Line Team, State Grid Jiaojiang Power Supply Company. Since October 2022, he has been conducting practical training in the transmission and inspection work area of State Grid Zhejiang Electric Power Supply Company, Taizhou Branch. He is responsible for the renovation project of the 110kV Zeyuan 1843 cable tower in Taizhou, and completed the implementation of the project.

XINYI HE was born Taizhou, Zhejiang, in February 1996. He received the bachelor's degree in electrical engineering and automation from the Shandong University of Technology, in 2018, and the master's degree in power electronics and power transmission from Shanghai Electric Power University, in 2021.

From 2021 to 2022, he was an Employee with the Substation Maintenance Center, State Grid Taizhou Power Supply Company. Since 2023, he has been an Employee with the State Grid Zhejiang Electric Power Supply Company, Taizhou Branch, Hongyuan Electric Power Design Institute, Hongchuang Group Company Ltd. His research direction is research on inverter control strategies. His academic situation, including the model predictive control based on geometric optimization of three sector voltage vectors; power electronics technology; multi resonant control of LCL grid connected inverter based on impedance analysis; power electronics technology; improved weighted average current control of LCL grid connected inverter and analysis of it order reduction characteristics; and *IET Generation, Transmission and Distribution.*